Elastomeric Polymers. 1. Application of Proton NMR Imaging to the Morphological Study of a Silicone Rubber

Maristella Gussoni,*,† Fulvia Greco,‡ Marina Mapelli,§ Alessandra Vezzoli,⊥ Elisabetta Ranucci,# Paolo Ferruti,# and Lucia Zetta‡

Dipartimento di Scienze e Tecnologie Biomediche, Università di Milano, Segrate (Mi), Italy; Istituto di Chimica delle Macromolecole, CNR, Milano, Italy; Istituto Oncologico Europeo, Milano, Italy; Ex Istituto di Tecnologie Biomediche Avanzate, CNR, Milano, Italy; and Dipartimento di Chimica Organica e Industriale, Università di Milano, Milano, Italy

Received July 30, 2001

ABSTRACT: Proton NMR imaging techniques were used to characterize a silicone rubber, intended mainly for biomedical applications, modified by an "in situ" polymerization. The study was aimed at the investigation of the effect of the polymerization on the silicone properties and of the dispersion of the guest polymer inside the host matrix. Before the onset of the reaction, the silicone, swollen either in water or in toluene, was characterized. Any source of inohomogeneities such as air bubbles or defects was localized and measured, and the geometry was recognized. By comparing the signal intensity from images collected before, during and after the polymerization reaction as well as the T_1 and T_2 relaxation time values, the guest polymer was found almost homogeneously dispersed in the host matrix, without preferential locations and/or agglomerates. The silicone network did not appear significantly altered by the presence of the guest polymer. The occurrence of the "in situ" polymerization reaction was proved by infrared spectroscopy.

1. Introduction

Contamination of biomedical polymeric materials with microorganisms has been up to now quite a serious problem, normally overcome by sterilization with steam, chemicals, and radiation. Self-sterilizing materials, endowed with intrinsic antimicrobial activity conferred by polycationic biocides, have been shown to be powerful candidates to solve this problem.[1] In particular, the use of antibacterial quaternary ammonium polymers, containing easily biodegradable backbones, has been previously described.[2−4] Among the seminorganic silicon-containing polymers, poly(dimethylsiloxane) (PDMS) has been shown to have physical properties very suitable for both medical and nonmedical applications.[5] Quaternary ammonium polymers have been "in situ" polymerized (guest polymer) by some of us[6] inside a preformed polymeric network of a commercial PDMS (host polymer), intended mainly for biomedical applications. The obtained material exhibited a good antimicrobial activity, even against usually resistant species.[6] The silicone rubbers obtained upon "in situ" polymerization showed that the guest polymer was apparently well dispersed within the host matrix and that the polymerization process did not appreciably affect the mechanical and dynamical properties of the silicone. Moreover, the presence of the guest polymer resulted in a significant decrease (about 5−7 °C) of the glass transition temperature (T_g) of the silicone rubber (−125 °C).[6] However, the localization of the guest polymer inside the host polymer, the quality of the dispersion, and the possible changes in the physical properties of silicones upon the "in situ" polymerization reaction still remained questionable. Therefore, we decided to employ the nuclear magnetic resonance imaging (NMRI) technique to get some new information on (i) the structure of the silicone matrix, mainly concerning the presence of air bubbles and/or defects; (ii) the effect of an "in situ" polymerization reaction on the intrinsic properties of the matrix; and (iii) the distribution of the guest polymer inside the silicone matrix.

Flourishing in the field of medicine, NMRI is also recognized as an important tool for nonmedical applications, especially in materials research.[7−10] Because of its sensitivity to molecular motions and chemical composition, NMRI is well-suited for the characterization of composite materials, which can be spatially mapped in a nondestructive and noninvasive manner. In NMRI the image contrast is produced by spatial variation of many parameters such as the proton density as well as the relaxation parameters T_1 and T_2.[11] Silicones are a peculiar class of solids characterized by a high chain segmental mobility, leading to a relaxation behavior that presents both liquidlike and solidlike components. The solidlike component is sensitive to cross-link density, stress, and strain.[12] At temperatures well above the glass transition temperature, T_g, the time scales and amplitudes of molecular motion are liquidlike. However, the chain motion is not isotropic: as a consequence, anisotropic spin interactions, such as dipole−dipole coupling, are not averaged to zero, giving rise to a solidlike behavior. Nevertheless, these residual dipolar interactions may be quite small compared to those in rigid solids; hence, the proton NMR line width for rubbery polymers, at about 100 °C above T_g, can be sufficiently sharp for imaging by standard techniques.[13] Indeed, by standard techniques, NMRI can reach reasonably high spatial resolution, even if resolution and sensitivity can be improved by techniques used in

† Dipartimento di Scienze e Tecnologie Biomediche, Università di Milano.
‡ Istituto di Chimica delle Macromolecole.
§ Istituto Oncologico Europeo.
⊥ Ex Istituto di Tecnologie Biomediche Avanzate.
Dipartimento di Chimica Organica e Industriale, Università di Milano.
* Corresponding author: e-mail Maristella.Gussoni@unimi.it; Fax +39-2-7064-3557.

10.1021/ma011355l CCC: $22.00
Published on Web 02/01/2002

Scheme 1. Polymerization Reaction

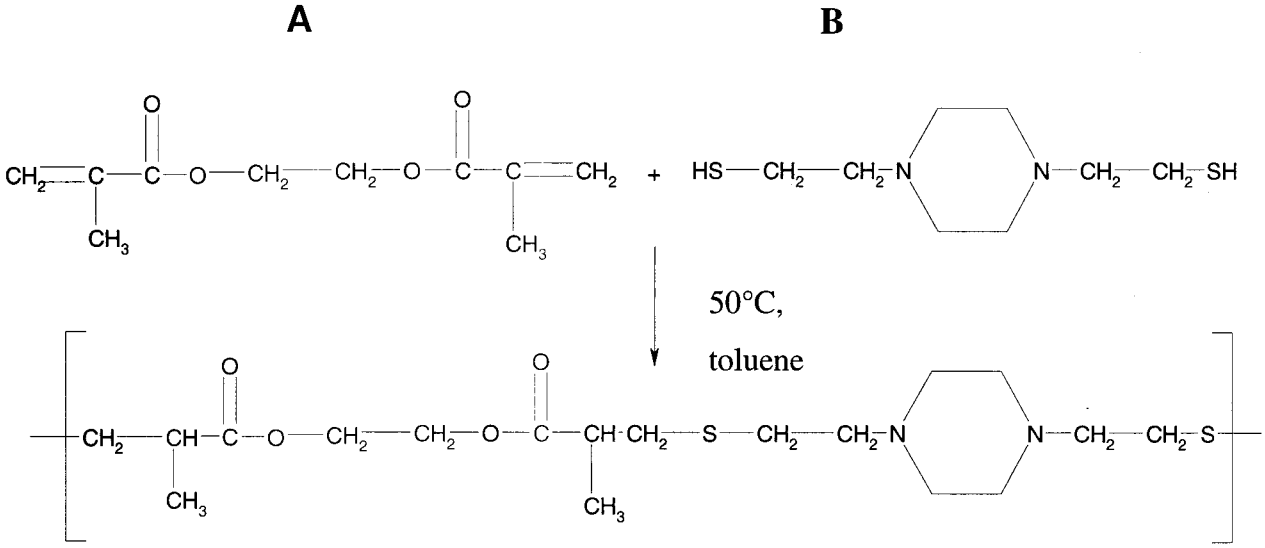

imaging solid materials, as, for instance, the STRAFI method.[9]

The main results of this study are (i) air bubbles and defects in the silicone matrix were localized, their size was measured, and the geometry was identified; (ii) the "in situ" polymerization reaction did not significantly modified the elastomeric properties of the silicone matrix; and (iii) the guest polymer was almost uniformly dispersed inside the host matrix.

2. Experimental Section

2.1. Materials. The study was carried out on SILS, a commercial silicone rubber, Siloprene HV, purchased from Bayer. The rubber was cured and filled with silica up to 40−50% (density 1.0−1.2 g cm^{-3}). SILS is thermally stable at temperatures higher than 350 °C and contains vinyl groups. It was characterized by an elemental analysis leading to the structure $(SiO(CH_3)_2)_n$.

Ethylene glycol dimethacrylate, piperazine, and ethylene sulfide were purchased from Fluka and used without further purification.

2.2. "In Situ" Polymerization. The procedure employed in the present study has been described in previous papers.[3,4,6] Scheme 1 shows two reactant monomers—A (ethylene glycol dimethacrylate) and B (1,4-piperazinediyldiethanethiol)—that by an addition reaction give poly(ester thioether amine), henceforth referred to as polyC. The silicone SILS was selected as matrix for the "in situ" polymerization reaction. The two monomers were dissolved, in equimolar amounts (15% w/v), in perdeuterated toluene in the NMR tube. Therefore, the reaction between A and B occurred in the NMR tube, and hence it could be followed by NMRI step by step (see below). The silicone was swollen in perdeuterated toluene containing the monomer mixture. Below room temperature and in aprotic solvents, the reaction rate of the monomers was found to be very slow. Hence, by keeping the reaction NMR tube at 0 °C, it was possible to swell the silicone in the presence of the reactant molecules, preventing the polymerization to occur outside the silicone matrix. Polymer formation was then induced by increasing the temperature up to 50 °C, under nitrogen, to avoid oxidation of the thiol groups. To allow the polymerization to proceed to completion, the reaction mixture was kept at this temperature for a few days, and then the rubber was dried to constant weight. For comparison and characterization purposes, polyC was prepared under the same conditions, but in the absence of the silicone matrix and then studied by NMRI.

2.3. NMRI and NMR Spectroscopy. NMRI and NMR experiments were carried out on a 4.7 T Bruker AM WB spectrometer equipped with a probehead tunable at the ^1H resonance frequency (200.13 MHz) and a gradient drive unit utilized for NMRI experiments. Orthogonal field gradient coils, built into the probehead, were capable of achieving gradients up to 50 G/cm, with a trigger pulse of 5 μs for switching the gradients. Since in this configuration the instrument was not provided with a field frequency stabilization (lock channel), at the beginning of each experiment the field frequency was set on the silicone methyl proton resonance that resulted about 50 Hz downfield from the tetramethylsilane (TMS) proton resonance. All experiments were carried out using a 15 mm insert and introducing the sample, 3 mm thick, into a 10 mm NMR tube. NMRI experiments were performed employing 2D phase/frequency encoding imaging spin-echo (SE) and gradient-echo (GE) sequences, standardly supplied by Bruker. A snapshot sequence was used to monitor the swelling process of the silicone. Matrices 256 × 256 were acquired with a pixel resolution of 86 × 86 μm^2 with 30 averages. One image was obtained in about 1 h. Acquisition parameters were spectral width of 100 kHz, echo delay time (TE) of 5.82 and 3.54 ms for SE and GE, respectively, and recycle time (TR) of 1 s. Thus, all the images were T_1 weighted in the same way. For the snapshot sequence an excitation soft pulse of less than 10 deg, a recycle time of 10 ms was used and an image was acquired with one average. Selective radio-frequency pulses (2000 Hz bandwidth, Gaussian-shaped, truncated at 5% level) were used. Other acquisition parameters are reported in the figure captions.

The longitudinal relaxation decay (T_1) of SILS was estimated using the inversion−recovery sequence and calculated with the supplied DISR89 Bruker software.

The transversal magnetization decay (T_2) was measured by the common Hahn spin-echo technique, which eliminates the inhomogeneities of the magnetic field and of the chemical shifts but does not influence the dipolar and quadrupolar interactions. The signal decay was fitted using the approximated equation proposed by Kuhn et al.,[14] consisting of a sum of a Gaussian and an exponential term that describe the solidlike and the liquidlike contribution to the transverse relaxation, respectively. The experimental data were fitted by the Marquardt−Levenberg algorithm implemented in the Sigma Plot software (Jandel).

2.4. IR Spectroscopy. Infrared spectra were acquired on a Jasco 5300 FT-IR spectrophotometer. IR measurements were performed on the SILS samples previously subjected to the "in situ" polymerization in the NMR tube. The principal infrared absorptions (cm^{-1}) in the spectra are the following: 2940, 2880, 2800, 2760: stretching C−H; 1720: stretching C=O; 1459: bending CH_2; 1260, 840, 750: stretching Si−$(CH_3)_2$;

1158: stretching CO−O; 1120: stretching C−N; 1010: stretching Si−O.

3. Results and Discussion

3.1. Silicone Characterization. The silicone matrices were characterized prior to polymerization as a negative control. Particular attention has been given to (i) the presence in the silicone of inhomogeneities such as internal bubbles and defects and (ii) the behavior of such inhomogeneities upon imbibition of the silicone rubbers with protic or deuterated solvents.

3.1.1. Defect Detection. Different sources of inhomogeneity could be found in commercial silicones such as the presence of air bubbles, of differently cross-linked regions, of entanglements, etc. The spatial localization of inhomogeneities within SILS samples has been visualized by NMRI images obtained by both SE and GE experiments. The dimensions of the defects can be calculated by SE images, while in GE images the defects appear with enhanced size. In fact, voids and defects cause variation of bulk susceptibility, inducing additional inhomogeneous line broadening. This broadening can be distinguished from the true relaxation by echo refocusing. In the echo produced by the SE sequence all the inhomogeneous broadening effects are refocused by the 180° soft pulse, so that the image is attenuated by T_2 relaxation. On the contrary, in the GE sequence, gradients are reversed, but the 180° pulse is not employed. This means that the inhomogeneous broadening continues to cause dephasing and the image is attenuated by T_2*. Thus, in the latter case, fine structures with macroscopic difference in magnetic susceptibility result in strong field inhomogeneities and appear with enhanced size. It must be pointed out that the size of the defects that could be detected was severely limited by the adopted slice thickness of 3 mm that was about 30 times larger than the adopted in plane resolution of 86 μm^2 (see captions of Figures 1−3). Therefore, the planar size of the defects could be accurately measured by the SE experiments, while their thickness might have been a substantial fraction of the real slice thickness.

The spin-echo (a) and gradient-echo (b) images of a piece of SILS are compared in Figure 1. The few defects, even if detectable in both images, are anyway better visible in the GE image, where two kinds of artifacts are present. The most important one shows up as a dark and bright ring pattern that could be correlated to the presence of one big and two small air bubbles. The former presents a diameter of about 500 μm, as calculated from the corresponding SE image. The other artifact enhances the contrast of the external border of the piece of silicone. According to several reports,[15−17] both kinds of artifacts are induced by the difference in magnetic susceptibility between polymer and air, and therefore they are absent in the SE images. Susceptibility effects are well-known in NMRI as inducing image artifacts and causing signal attenuation in the presence of molecular motion. The functional form of the spatial dependent susceptibility ($\chi_m(r)$) depends both on the sample geometry and on the direction of the applied magnetic field, normal or transverse to the slice plane. Local susceptibility-related gradients, which may become very large in the vicinity of small susceptibility inhomogeneities, lead to additional spatially dependent signal losses due to gradient-echo phase shifts and to diffusion, so modifying the image contrast at susceptibility interfaces. It was demonstrated that GE technique suffers much stronger signal losses than the SE technique, even at relatively short echo times. On the other hand, GE technique introduces strong image intensity variations around strong local-field distortions. These intensity variations are due to the spread-out of pixel information from regions with different spin phases. This effect is not present in spin-echo images, where the spin phase in the sample is uniform.[16] Intensity and phase pattern leading to this kind of artifacts have been calculated[15] and proved to be sensitive parameters for the characterization of the geometry of the defect. The artifact due to air bubbles, localized in the interior of the silicone, without connections with the exterior (see below), resulted to be typical of a spherical defect. To confirm this hypothesis, a phantom was prepared with a spherical defect of known shape and bulk magnetic susceptibility difference ($\Delta\chi_{m(water-air)} \sim -9.05 \times 10^{-6}$). An air-filled glass capillary tube, sealed on the top and endowed with a spherical cavity (diameter of about 1.6 mm) at the bottom, was inserted coaxially into a 10 mm NMR tube filled with water. Figure 2 shows the images of the phantom obtained by spin-echo (a) and gradient-echo (b) sequences. In Figure 2a the void due to the spherical cavity appears with its real size, while in Figure 2b the cavity size is magnified and the expected alternate dark and bright rings can be observed.

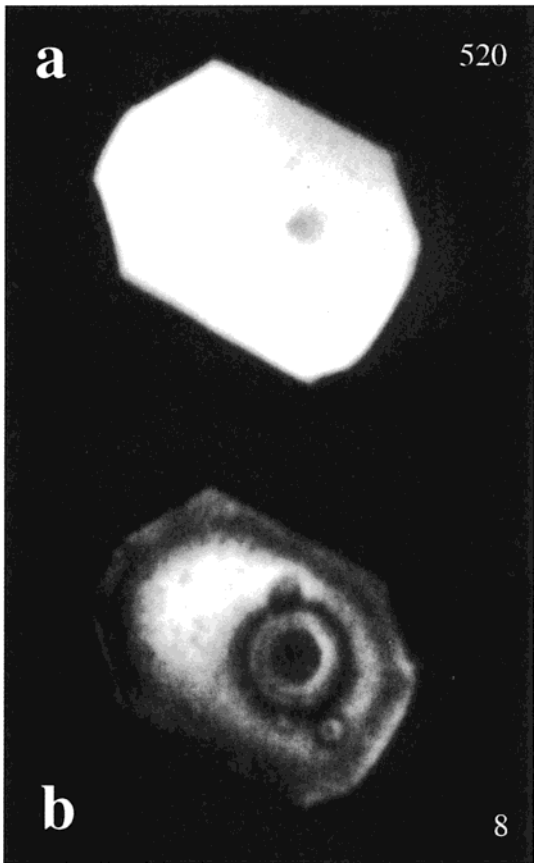

Figure 1. Images of commercial silicone, Silopren HV (SILS, with silica). Transversal slices from (a) spin-echo and (b) gradient-echo images. *xy*-field of view (FOV): 11 mm; voxel resolution: 86 × 86 × 3000 μm^3. Averages (NE) = 30; TR = 1 s; receiver gain (RG) = 40. (a) rf hard 90° pulse ($\pi/2$) = 13.3 μs; TE = 5.82 ms. (b) rf soft 90° pulse ($\pi/2$) = 512 μs; TE = 3.54 ms.

3.1.2. Swelling Properties. Diffusion and sorption of small molecules are important processes to study silicone polymer properties from the production stage

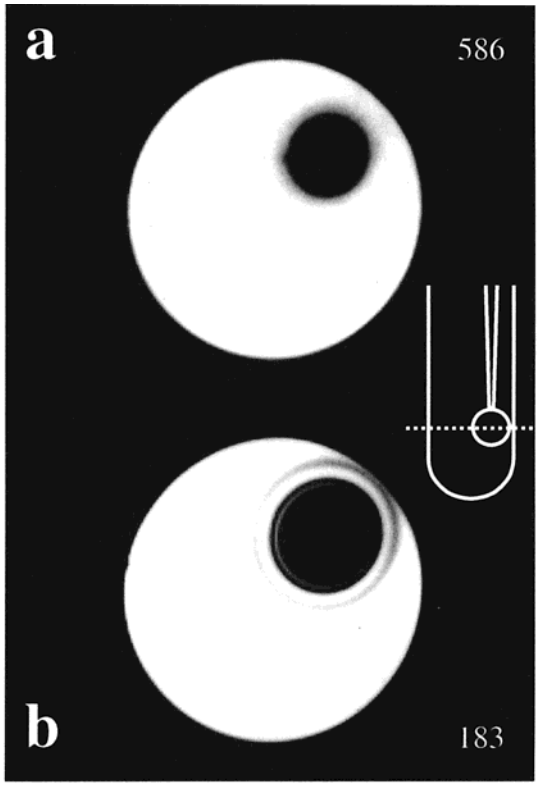

Figure 2. Transversal images of an air-filled glass capillary tube, endowed with a spherical cavity at the bottom, inserted coaxially into a water-filled 10 mm NMR tube. On the right side of the figure a schematic representation of the phantom is reported. The horizontal dotted line indicates the position of the center of the receiver coils in correspondence of the air cavity. (a) Spin-echo and (b) gradient-echo images. *xy*-field of view (FOV): 11 mm; voxel resolution: 86 × 86 × 3000 μm^3; TR = 1 s; RG = 4; NE = 30. (a) rf hard 90° pulse ($\pi/2$) = 12.8 μs; TE = 5.82 ms. (b) rf soft 90° pulse ($\pi/2$) = 512 μs; TE = 3.54 ms.

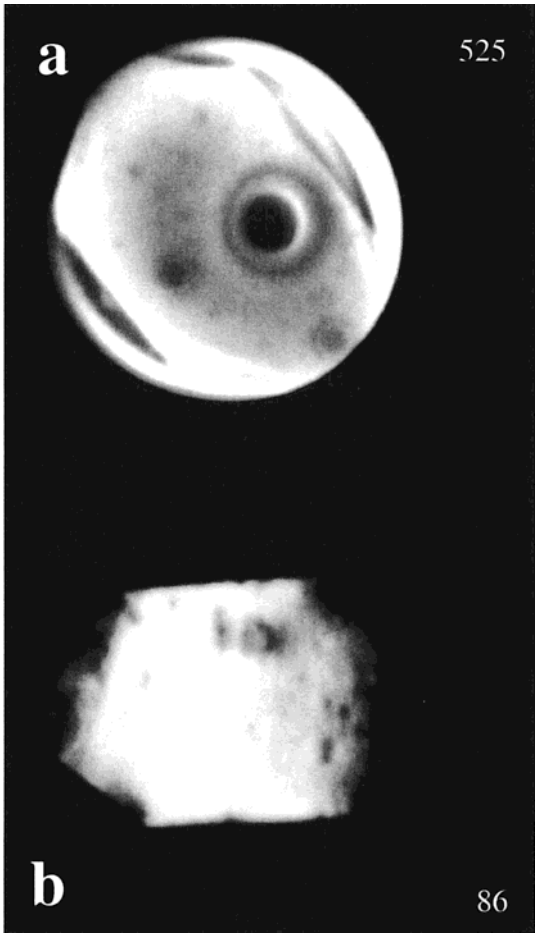

Figure 3. Transversal images from gradient-echo experiments of a piece of SILS (a) embedded in water and (b) swollen in perdeuterated toluene. *xy*-field of view (FOV): 11 mm; voxel resolution: 86 × 86 × 3000 μm^3; NE = 30; TR = 1 s. (a) rf soft 90° pulse ($\pi/2$) = 512 μs; RG = 20; TE = 3.54 ms. (b) rf soft 90° pulse ($\pi/2$) = 512 μs; RG = 16; TE = 3.54 ms.

to the final use. Macroscopic properties of rubbers, like cross-link density, strongly affect the swelling processes and hence the relaxation parameters that influence the image contrast of a swollen material.[18,19] NMR imaging is primarily sensitive to protons in mobile solvent molecules, and hence it is particularly well-suited for studying diffusion processes as well as to directly detect inhomogeneities within the samples in a noninvasive manner.[20]

The swelling properties of SILS indicated that both toluene and chloroform provided convenient solvent systems to swell the silicone and to dissolve the monomeric mixture selected for the "in situ" polymerization. However, toluene was preferred because of its superior chemical stability and lower volatility. Moreover, in the experiments aimed at imaging the proton density of the rubber material, samples have been swollen in perdeuterated solvent. On the contrary, water did not swell the silicone neither diffused into it: for these two reasons it could be used to localize defects of various sizes and shapes such as voids and inhomogeneities.

The swelling properties of the silicone are presented in Figure 3, which shows the GE images of the same piece of SILS of Figure 1 embedded both in water (a) and in perdeuterated toluene (b). No morphological changes in the material were observed in water. The SE image (not shown) was not very significant, due to the poor difference in contrast between water and silicone. On the contrary, the GE image (Figure 3a) clearly demonstrates that the voids are still empty and hence inside the silicone, not communicating with water. The same image shows that the artifacts observed in Figure 1b at the border of the silicone result strongly reduced. This was expected, since the susceptibility difference between silicone and water is lower than that between silicone and air. The same piece of silicone was then embedded in perdeuterated toluene in order to image mainly the silicone proton density. Upon swelling, a substantial variation of the sample morphology is observed (Figure 3b). The silicone strongly swelled, increasing its volume and changing its shape. The cavities containing air, shown in Figures 1 and 3a, completely disappeared in both spin-echo (not shown) and gradient-echo (Figure 3b) images. In the latter the alternate dark and bright artifacts (Figure 1b) are no more observable, and as already observed in water (Figure 3a), also the artifacts caused by the silicone−air interface (Figure 1b) are strongly reduced, indicating that air was substituted by toluene. On the other hand, by acquiring the proton signal of a fluid diffusing into the polymer matrix, it is possible to map the spatial distribution of the solvent during the time course of the swelling process. Therefore, another bar of SILS was embedded in protonated toluene, and the swelling process was followed by using a snapshot sequence for obtaining proton density image of both the silicone and the solvent. For the snapshot imaging method, based

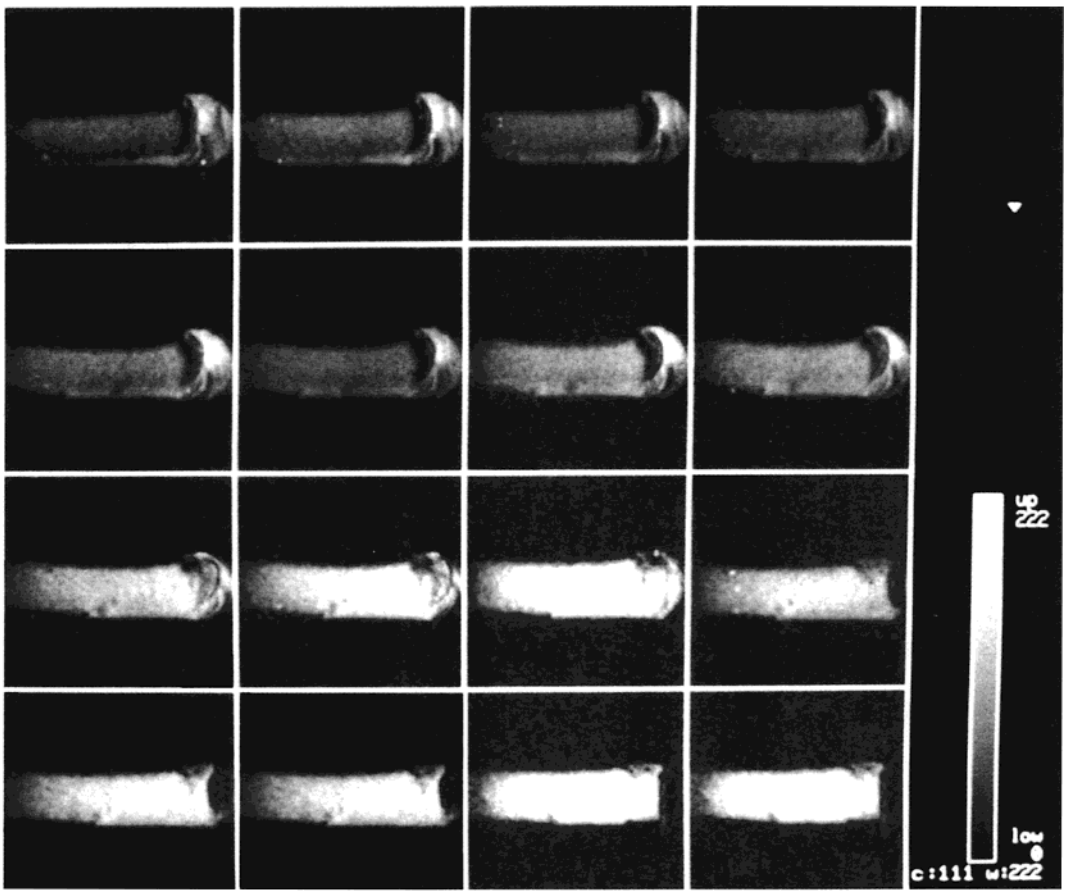

Figure 4. Swelling process of SILS in toluene. Longitudinal slices from snapshot experiments. *z*-field of view (FOV): 30 mm; voxel resolution: 235 × 235 × 3000 μm^3. The tube appears tilted in all images. Toluene is at the bottom of the tube, which is on the right side of each image and disappears during the time course of the experiment (see text). The images were collected during the swelling process at (from the top to the bottom and from the left to the right side): 1st row (1−4 frame**)**: 0 min (beginning of the experiment), 2 min, 4 min, 8 min; 2nd row (5−8 frame): 10 min, 20 min, 30 min, 1 h; 3rd row (9−12 frame**)**: 3 h, 5 h, 9 h, 11 h; 4th row (13−16 frame): 13 h, 15 h, 19 h, 20 h. RG = 16; NE = 1; TE = 3.54 ms; TR = 10 ms.

on GE data acquisition method,[21] a very short excitation soft pulse can be used, so employing a very short repetition time. Moreover, the acquired imaging data are collected in an array and put in the Fourier transforming 2D matrix by a procedure performed at the end of the acquisition experiment. The pulse sequence is very fast, and strong gradients may be used, obtaining an image in a single average. Therefore, the snapshot imaging method is well-suited to monitor processes like the swelling of the silicone bar. Figure 4 shows spatially resolved maps of the diffusion process through the silicone bar: at the beginning, toluene is visible at the bottom of the NMR tube. The brighter contrast of toluene, with respect to the silicone bar, is due to the long T_2 associated with the molecular motion of the liquid. The delays between two consecutive acquisitions were incremented from 2 min to 1 h, following the observed decrease in the swelling rate. After 30 min from the beginning of the experiment (first frame, see figure caption), the silicone bar becomes slightly brighter and increases its volume. The front of toluene progresses through the bar between 3 and 5 h and between 5 and 9 h. At this time, the meniscus of the solvent seems to be almost completely disappeared from the bottom of the tube. After about 20 h, toluene appears almost homogeneously distributed inside the bar, which shows up with a higher intensity and an increased volume with respect to the beginning of the experiment. Therefore, the use of the snapshot imaging method and protonated toluene allowed to follow the progression of the solvent front that even at room temperature was found very slow and not linearly related to the swelling time. All these findings well characterized the matrix in order to better assess possible changes in the matrix properties as a consequence of the polymerization reaction directly induced in the NMR tube (see section 3.3).

3.2. Polymer Characterization. PolyC, the guest polymer, prepared in the absence of the silicone matrix could not give NMRI signal, most likely due to its T_2, too short if compared to the echo-time scale used for imaging. In fact, as shown in Figure 5, a layer of polyC, interposed between the two pieces of SILS appearing in the figure, results completely dark.

3.3. "In Situ" Polymerization. It is well-known that the properties of a silicone rubber depend strongly on the dispersion of guest components and on the cross-link contents. Silicones with good or poor silica dispersions, without silica filler or endowed with a different content in cross-links, are expected to produce different NMR images. It is also known that an inhomogeneous spatial distribution of filler particles or guest polymers within elastomeric matrixes can produce locally a reduced molecular mobility which is reflected in the local relaxation rates.[22] Thus, in order to properly study the distribution of polyC in the silicone matrix, in addition to the local cross-link content, the presence of two kinds of "rigid" agglomerates has been taken into account as possible cause of susceptibility artifacts: domains of polymer as well as of silica. The polymeri-

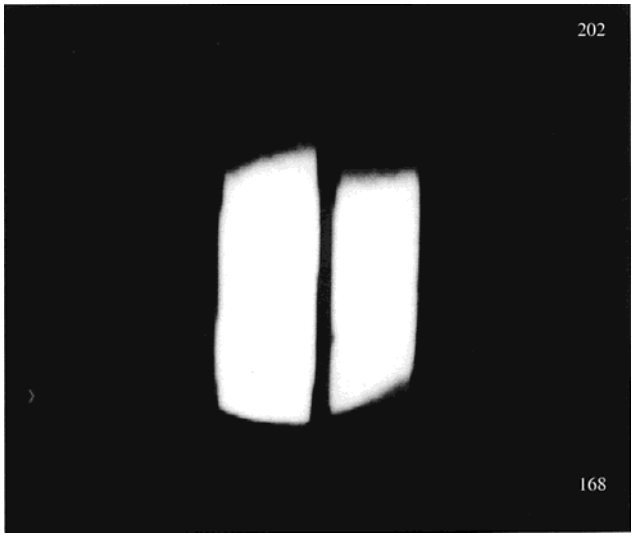

Figure 5. Layer of polyC interposed between two pieces of SILS. Longitudinal slice from a spin-echo experiment. *z*-field of view (FOV): 10 mm; voxel resolution 78 × 78 × 3000 μm^3; RG = 20; NE = 300; TE = 5.81 ms; TR = 1 s.

zation process, induced in the NMR tube, was followed on the same SILS sample, keeping the same NMR acquisition parameters, to be able to compare each phase of the process and to rationalize possible changes in light and dark contrast as well as to identify preexisting rigid aggregates of silica. We were confident that gradient echo images, which are sensitive to local variances in relaxation properties, could give an inhomogeneous view of the samples, even if the microscopic guest domains were below the spatial resolution. Therefore, GE was the method of choice to study the polymerization reaction.

Figures 6 and 7 show spin-echo and gradient-echo images collected in order to follow the polymerization process step by step. Figure 6 shows spin-echo and gradient-echo images collected before the onset of the "in situ" polymerization reaction at room temperature (Figure 6a,b) and at 50 °C (Figure 6c,d). They were used as a reference for the analysis of the successive steps of the process. The images were collected at the pixel resolution used for all previous images, but a slice thickness of 500 μm was chosen to reach a better voxel resolution. At the same time, the S/N ratio improved about 3 times by increasing the number of averages (NE = 300), and the images were collected in about 10 h. As expected, the piece of silicone shows homogeneous spin-echo images (Figure 6a,c) and highly differentiated gradient echoes (Figure 6b,d). The latter ones are characterized by a wide dark contrast in the middle of the bar and by a few little and localized dark inohomogeneities. At 50 °C the images (Figure 6c,d) appear brighter than those collected at room temperature due to a higher chain mobility of the elastomeric network. At this temperature also the contrast between the dark localized domains and the matrix improves in GE images. These findings indicate that SILS presents

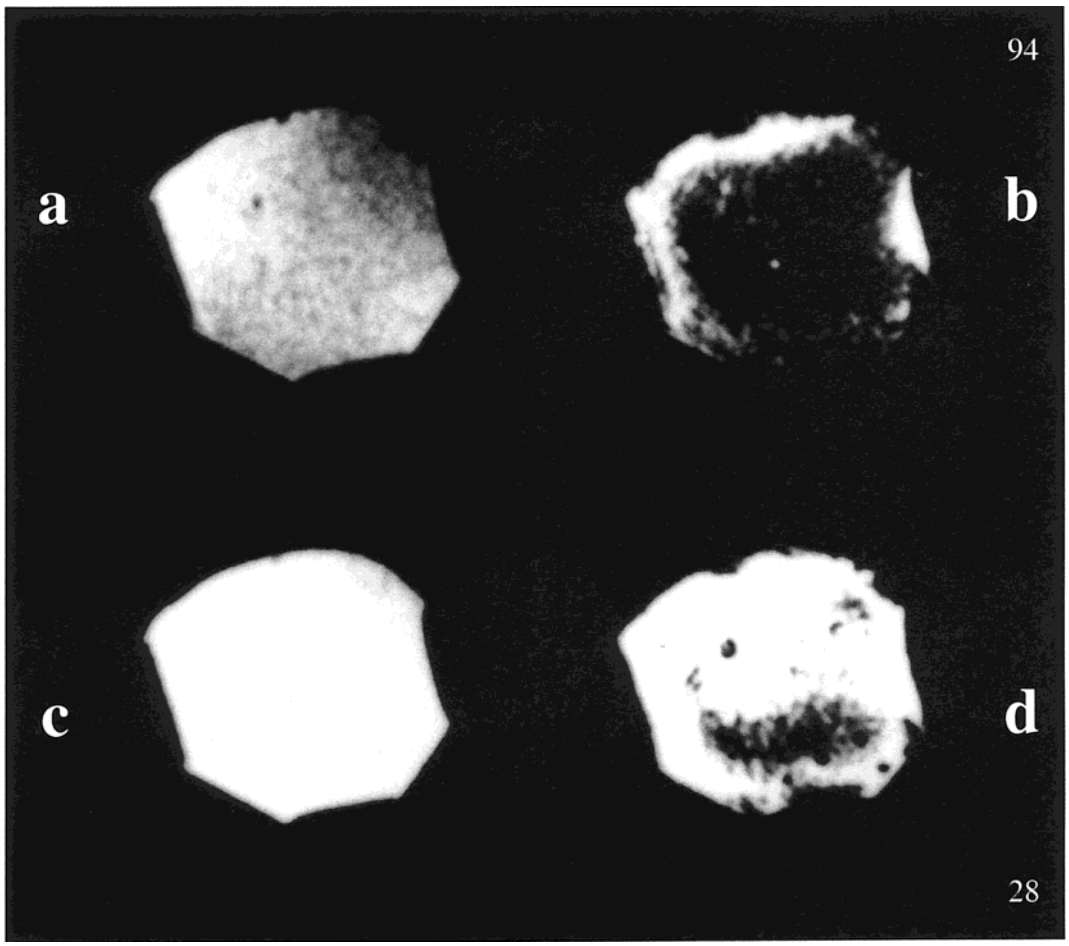

Figure 6. Spin-echo (a, c) and gradient-echo (b, d) images of SILS collected before the onset of the "in situ" polymerization reaction: at room temperature (a, b) and at 50 °C (c, d). *xy*-field of view (FOV): 11 mm; voxel resolution 86 × 86 × 500 μm^3; NE = 300; TR = 1 s. (a, c): $\pi/2$ = 18.3 μs; RG = 200; TE = 5.82 ms. (b, d): rf soft 90° pulse ($\pi/2$) = 512 μs; RG = 400; TE = 3.54 ms.

Figure 7. Gradient-echo images collected (a) at 0 °C during the swelling process of SILS and (b) at 50 °C after the polymerization reaction. *xy*-field of view (FOV): 11 mm; voxel resolution 86 × 86 × 500 μm^3; RG = 200; NE = 300; TE = 3.54 ms; TR = 1 s.

intrinsic local inhomogeneities, characterized by different T_2*, which should not be assigned to the polymerization process. The bar was then swollen in perdeuterated toluene at 0 °C, in the presence of the two monomers. Figure 7a shows the gradient-echo image collected when the bar was not yet completely swollen, as suggested by the presence of two different regions. The brightest one corresponds to the region where toluene has already been absorbed while the darkest one corresponds to the part still dry. The isotopic impurity of perdeuterated toluene can be better observed on the walls of the NMR tube. As expected, a quite different image contrast is observed after the swelling than before (Figure 6b). Several overlapping factors contributed to the local changes in the contrast. The intensity increasing factors were (i) the higher segmental mobility of the piece of silicone deriving from the swelling process, (ii) the presence of the solvent isotopic impurity, and (iii) the presence of the two monomers dissolved into it. The very low temperature (0 °C) adopted during the imaging experiment was mainly taken into account as intensity decreasing factor. In fact, since the experimental temperature was not enough above the silicone T_g, some elastomeric properties could have been lost.

The sample was then warmed to 50 °C and kept at this temperature for 7 days, to be sure that the reaction process was completed and to let the toluene evaporate completely. At the end of this period, images were collected. A gradient-echo image collected at this stage is shown in Figure 7b. It appears more homogeneous than the reference one (Figure 6d), most likely due to the swelling procedure that eliminated defects, such as voids or bubbles, before the onset of the polymerization process. The dark contrast at the border of the bar is still observable, but no additional artifacts can be detected. This result indicates the absence of preferential localizations of polyC, which otherwise should have produced additional local contrast arising from the magnetic susceptibility difference between the silicone matrix and the guest polymer.

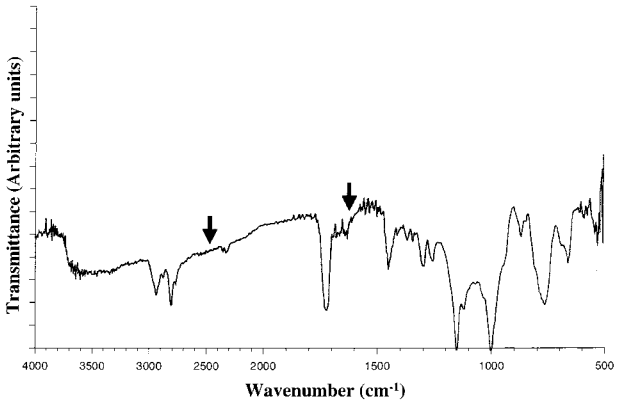

Figure 8. FT-IR spectrum of SILS after the "in situ" polymerization. The presence of both polyC and SILS is demonstrated by the diagnostic bands (cm^{-1}) (see the Experimental Section). In particular, the bands at 1720 cm^{-1} ($\nu_{C=O}$) and 1158 cm^{-1} (ν_{CO-O}) confirm the presence of polyC. The absence of the bands of the reactive functions of the two monomers are indicated by an arrow (see text): ethylene glycol dimethacrylate at 1639 cm^{-1} ($\nu_{C=C}$) and 1,4-piperazinediyldiethanthiol at 2600−2550 cm^{-1} (ν_{S-H}).

To support the imaging data, T_1 and T_2 relaxation time measurements were carried out on the bar of SILS before and after the polymerization process induced in the NMR tube (see above). T_2 data were fitted as described in the Experimental Section. After the polymerization process, the longitudinal relaxation time values (T_1) did not significantly change: its mean value calculated between the T_1's derived before and after the reaction on the same sample used also for the NMRI experiments resulted 1.07 ± 0.21 s. On the other hand, on the same sample, a transversal relaxation time (T_2) of 5.73 ms was calculated before the reaction. After the polymerization it was slightly shorter, resulting 4.43 ms. Therefore, T_1 and T_2 relaxation values indicate, in agreement with imaging data, that the elastomeric network was not substantially affected by the polymerization reaction.[23]

The occurrence of the "in situ" polymerization reaction was proved by infrared spectroscopy. Figure 8 shows the FT-IR spectrum of the SILS polymerized in the NMR tube. The IR spectrum of the silopren−polymer adduct confirmed that the polymerization reaction between ethylene glycol dimethacrylate and 1,4-piperazinediyldiethanthiol had actually taken place inside the swollen rubber. The above-cited spectrum shows in fact diagnostic bands of both silicone matrix (in particular, Si−O stretching at 1010 cm^{-1} and $Si(CH_3)_2$ fingerprints at 1260, 840, and 750 cm^{-1}) and polyC (in particular, C=O stretching at 1720 cm^{-1} and CO−O stretching at 1158 cm^{-1}). On the other hand, no evidence is given of diagnostic bands (arrowed in the spectrum) of those monomer functions that are expected to disappear as a

consequence of polymerization (in particular, C=C stretching at 1639 cm^{-1} for ethylene glycol dimethacrylate and S−H stretching at 2600−2550 cm^{-1} for 1,4-piperazinediyldiethanthiol).

4. Conclusions

The morphological characterization of a silicone rubber has been obtained before and after an "in situ"polymerization reaction, by using both spin-echo and gradient-echo NMRI techniques. Possible defects present in the silicone samples such as voids or bubbles were localized and described in shape and size. It was demonstrated that possible inhomogeneities were completely eliminated by the swelling procedure with toluene. This was a very important point to conclude that, upon polymerization, polymer domains were the only possible source of inhomogeneities, assuming that the distribution of cross-links and silica filler has been kept constant. The only possible side reaction that could occur was the formation of new cross-links due to thermal aging,[24] as the sample was kept at 50 °C for a few days. Indeed, the longitudinal relaxation time was practically insensitive to the polymerization reaction, while the spin−spin relaxation time was found slightly shorter upon polymerization (5.73 ms before and 4.43 ms after polymerization).

Comparison of gradient-echo images collected before and after the polymerization process at the same temperature of 50 °C did not show appreciable changes in light and dark contrast, suggesting a homogeneous distribution of the guest polymer within the host matrix. This finding is consistent with the results obtained with calorimetric experiments carried out on SILS upon polymerization.[6] Differential scanning calorimetric tests performed under different conditions never displayed separate transition phenomena and showed a significant decrease (about 5−7 °C) of the silicone glass transition temperature, indicating full miscibility of the two polymers in the studied range of composition.

Our results obtained by the NMRI technique could enrich the previous knowledge of the same "in situ" polymerization reaction by adding information on the absence of significant changes of matrix properties and on the spatial distribution of the guest polymer. Images showed that it is homogeneously distributed and not confined only on the surface of the sample. Even if the guest polymer shows its effect at the surface of the matrix, the presence of the polymer also in the interior of the bar ensures that, when the surface polymer is released, other polymer can be recalled to the surface, keeping the antibacterial properties of the material constant for a long time.

Acknowledgment. The authors express their grateful thanks to the "Fondazione Antonio de Marco" and the Italian National Research Council "Progetto Finalizzato Materiali Speciali per Tecnologie Avanzate II-Elastomeri" for financial support.

References and Notes

(1) Ikeda, T. In *High Performance Biomaterials. A Comprehensive Guide to Medical and Pharmaceutical Applications;* Szycher, M., Ed.; Technomics: Basel, 1991; p 743.
(2) Ferruti, P.; Ranucci, E. *Makromol. Chem. Rapid Commun.* **1987**, *8*, 549.
(3) Ranucci, E.; Ferruti, P.; Neri, M. G. *J. Bioact. Compatible Polym.* **1989**, *4*, 403.
(4) Ranucci, E.; Ferruti, P.; Neri, M. G. *J. Biomater. Sci. Polym. Ed.* **1991**, *2*, 255.
(5) Mark, J. E. *Adv. Chem. Ser.* **1990**, *224*, 47.
(6) Ranucci, E.; Ferruti, P.; Della Volpe, C.; Migliaresi, C. *Polymer* **1994**, *35*, 557.
(7) Jezzard, P.; Wiggins, C. J.; Carpenter, A. T.; Hall, L. D.; Jackson, P.; Clayden, N. J.; Walton, N. J. *Adv. Mater.* **1992**, *4*, 82.
(8) Blümich, B.; Blümler, P. *Macromol. Symp.* **1994**, *87*, 187.
(9) Miller, J. B. *Prog. Nucl. Magn. Reson. Spectrosc.* **1998**, *33*, 273.
(10) Blümich, B.; Blümler, P.; Gasper, L.; Guthausen, A.; Göbbels, V.; Laukemper-Ostendorf, S.; Unseld, K.; Zimmer, G. *Macromol. Symp.* **1999**, *141*, 83.
(11) Blümich, B. *Concepts Magn. Reson.* **1998**, *10*, 19.
(12) Sotta, P.; Fülber, C.; Demco, D. E.; Blümich, B.; Spiess, H. W. *Macromolecules* **1996**, *29*, 6222.
(13) Chang, C.; Komoroski, R. A. *Macromolecules* **1989**, *22*, 600.
(14) Kuhn, W.; Barth, P.; Hafner, S.; Simon, G.; Schneider, H. *Macromolecules* **1994**, *27*, 5773.
(15) Callaghan, P. T. *J. Magn. Reson.* **1990**, *87*, 304.
(16) Posse, S.; Aue, W. P. *J. Magn. Reson.* **1990**, *88*, 473.
(17) Bakker, C. J. C.; Bhagwandien, R.; Moerland, M. A.; Fuderer, M. *Magn. Reson. Imaging* **1993**, *11*, 539.
(18) Menge, H.; Hotopf, S.; Pönitzsch, S.; Richter, S.; Arndt, K.; Schneider, H.; Heuert, U. *Polymer* **1999**, *40*, 5303.
(19) George, S. C.; Knörgen, M.; Thomas, S. *J. Membr. Sci.* **1999**, *163*, 1.
(20) Webb, A. G.; Jezzard, P.; Hall, L. D.; Ng, S. *Polym. Commun.* **1989**, *30*, 363.
(21) Haase, A. *Magn Reson. Med.* **1990**, *13*, 77.
(22) Blümler, P.; Blümich, B. *Rubber Chem. Technol. Rubber Rev.* **1997**, *70*, 468.
(23) Gussoni, M.; Greco, F.; Mapelli, M.; Vezzoli, A.; Ranucci, E.; Ferruti, P.; Zetta, L. *Macromolecules* **2002**, *35*, 1722.
(24) Knörgen, M.; Heuert, U.; Menge, H.; Schneider, H. *Angew. Makromol. Chem.* **1998**, *261/262*, 123.

MA011355L